Stability of Interfacial Nanobubbles

Xuehua Zhang,*,[†] Derek Y. C. Chan,[‡,§] Dayang Wang,[∥] and Nobuo Maeda[⊥]

[†]Department of Chemical and Biomolecular Engineering and [‡]Department of Mathematics and Statistics, University of Melbourne, Melbourne VIC 3010, Australia

[§]Faculty of Life and social Sciences, Swinburne University of Technology, Hawthorn VIC 3122, Australia

[∥]Ian Wark Research Institute, University of South Australia, Adelaide SA 5095, Australia

[⊥]CSIRO Materials Science & Engineering, Ian Wark Laboratory, Bayview Avenue, Clayton, VIC 3168, Australia

ABSTRACT: Interfacial nanobubbles (INBs) on a solid surface in contact with water have drawn widespread research interest. Although several theoretical models have been proposed to explain their apparent long lifetimes, the underlying mechanism still remains in dispute. In this work, the morphological evolution of INBs was examined in air-equilibrated and partially degassed water with the use of atomic force microscopy (AFM). Our results show that (1) INBs shrank in the partially degassed water while they grew slightly in the air-equilibrated water, (2) the three-phase boundary of the INBs was pinned during the morphological evolution of the INBs. Our analyses show that (1) the lifetime of INBs was sensitive to the saturation level of dissolved gases in the surrounding water, especially when the concentration of dissolved gases was close to saturation, and (2) the pinning of the three-phase boundary could significantly slow down the kinetics of both the growth and the shrinkage of the INBs. We developed a one-dimensional version of the Epstein−Plesset model of gas diffusion to account for the effect of pinning.

Shrinking Nanobubble

Substrate

H↓; $L/2$ constant; Vol. ↓, $P_{(Laplace)}$ ↓
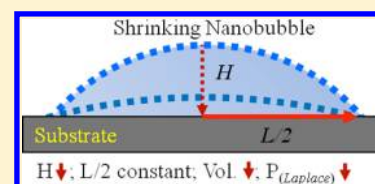
INTRODUCTION

The presence of interfacial nanobubbles (INBs) on a solid surface in contact with water is of importance in many processes.[1−4] For instance, INBs may enhance the attractions between two surfaces in water,[5,6] give rise to hydrodynamic slip against a solid wall,[7] initiate rupture of thin liquid films,[8] and facilitate macroscopic bubble attachment onto a solid surface.[9] Experimental measurements demonstrated that INBs can remain on the interface for hours or days after their formation.[10,11] However, the underlying mechanism for their stability is still an open question.

Theoretical prediction has been that bubbles at nanoscale dissolve very quickly due to the fast kinetics of gas dissolution into the surrounding aqueous phase, which is driven by high Laplace pressures.[12] Although the gas pressure inside INBs was measured to be only around 1.4 atm,[11,13] the experimentally observed lifetimes of INBs was surprisingly long. Attard, and later Ducker, proposed that an impermeable 'skin' prevented gas leaking out from the INBs.[14−17] However, our latest work showed that this mechanism is highly unlikely.[18] Lohse et al. proposed that gas diffusion into INBs to compensate for gas diffusion out of INBs, that is, INBs are in dynamic steady state.[19,20] The difficulty with this hypothesis is the lack of a source of the energy required for such gas flows. To gain insight into the stability mechanisms of INBs, in this work we studied the effects of the saturation level of dissolved air on the morphology of INBs with time. Our results clearly demonstrate the significance of gas saturation for the stability of INBs.

MATERIALS AND METHODS

1. Formation and Characterization of INBs. The substrates were decanethiol-coated gold surfaces. The RMS roughness of the surface was 1.8 nm over 5 μm × 5 μm. The advancing and receding contact angles measured using macroscopic water drops on the surface were 110° and 95°, respectively.

Atomic force microscopy (AFM) was used to reveal the detailed morphology of INBs in situ. The set point (amplitude/free amplitude) for tapping mode imaging was >0.98, scan rate 10 μm/s, and nominal tip radius 10 nm. The tip was treated by UV/ozone for 15 min before use. All images presented here were recorded by the same AFM tip using the same imaging parameters. The uncertainty of ±20 nm could be expected in the lateral size of INBs due to tip convolution. However, the *change* in the size of INBs with time could be detected with accuracy because any effects due to such distortions would cancel out.[21,22]

For identification of the central cross-sectional profile of an INB and the best fit of the spherical-cap shape, images were processed with custom-written software. The height (H) and lateral size (L) of INBs were measured from the original images. Radii of curvature of the INBs were evaluated from the fitting of the spherical cap, from which the Laplace pressure was calculated.

2. Stability of INBs with Gas Saturation. INBs were generated in the air-equilibrated water via the solvent exchange procedure described in our previous work.[11,13,23−25] Afterward, the preformed INBs were incubated in water with two different saturation levels of dissolved air. In one set of experiments, water was effectively supersaturated with air (see below); we refer to this water as "water$_{(H)}$". In the other set of experiments, water was predegassed before use and the gas saturation level was lower; we refer to this water
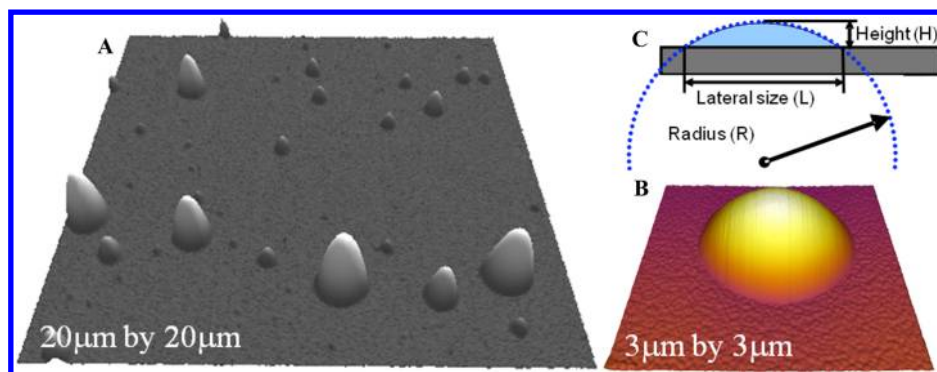
Figure 1. Morphology of interfacial nanobubbles (INBs). AFM image of INBs in air-equilibrated water (A), enlarged image (B), and schematic picture of an INB (C). Schematic picture defines key parameters that characterize the INB; height, H, lateral size, L, and mean radius of curvature of the interface, R.
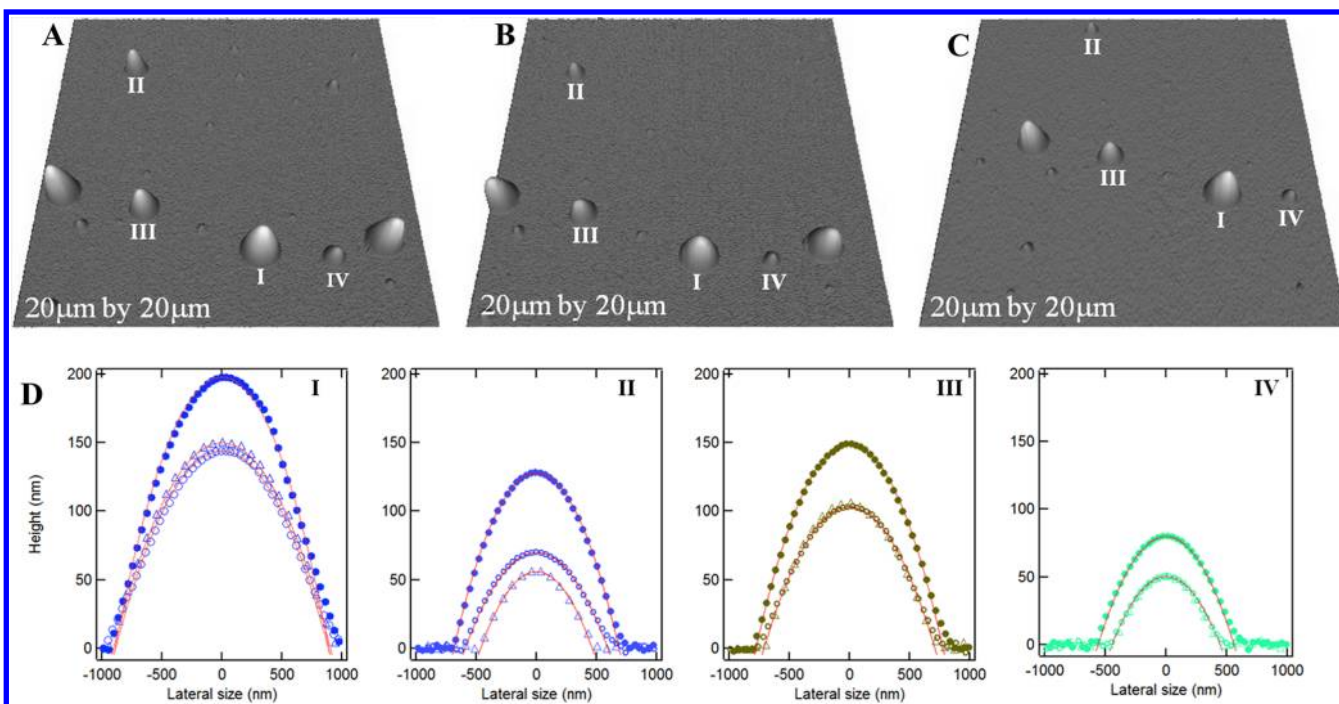

Figure 2. Morphology of interfacial nanobubbles (INBs) during incubation in water$_{(L)}$. (A−C) Incubation time was 0.25 h (A), 14 h (B), and 20 h (C). (D) Representative cross-sectional profiles of INBs after incubation in water$_{(L)}$. Incubation time was 0.25 (●), 14 (○), and 20 h (△). Profile of each INB was fitted with a spherical cap (solid line).

as "water$_{(L)}$". To prepare water$_{(H)}$, water was produced from a Mill-Q unit and kept at 4 °C overnight before it was slowly warmed up to the temperature in the lab, 22 °C. Water$_{(L)}$ was obtained by stirring water$_{(H)}$ under a reduced pressure of ∼80 kPa for 12 h at 22 °C.

In both sets of experiments, once in the fluid cell of atomic force microscope (MFP-3D, Asylum Research), the temperature of the water had risen to 30−32 °C (measured by a thermocouple) in less than 10 min because of the unavoidable heating from the AFM head and the small heat capacity of the cell. Such temperature rise had a significant influence on the saturation level of dissolved air in water.[26,27] The saturation level in the as-prepared water$_{(L)}$ and water$_{(H)}$ at 32 °C was estimated as given below.[26,27]

3. Estimation of Gas Saturation Levels. The saturation level, $f \equiv C_i/C_s$, is defined as the ratio of the actual dissolved gas concentration in water (C_i) to the concentration at saturation (C_s). $C_{(H)}$ is for water$_{(H)}$; $C_{(L)}$ is for water$_{(L)}$. We approximate the composition of air with a binary mixture of nitrogen and oxygen. The solubility of nitrogen and oxygen in water at 101 KPa at 22 and 32 °C was calculated by interpolation from the literature values that were available for selected temperatures.[27] Water was assumed to be fully

saturated at 22 °C prior to introduction to the AFM fluid cell, so $C_{i(H)}(22 \text{ °C}) = C_s(22 \text{ °C})$. For the degassed water, the gas concentration at 22 °C, $C_{i(L)}(22 \text{ °C})$, was calculated from $C_s(22 \text{ °C})$ using Henry's law. The fluid cell was closed, so the the total amount of gas in the cell was assumed to remain conserved during the temperature rise from 22 to 32 °C. We used the following composition for the calculation: 21% oxygen and 79% nitrogen.

$$C_{i(H)}(32°C) = C_{i(H)}(22°C) = C_S(22°C)$$

$$= 1.5 \times 10^{-5} \text{ (in mole fraction)}$$

$$C_{i(L)}(32°C) = C_{i(L)}(22°C) = C_{i(H)}(22°C) \times (80 \text{ kPa}/101 \text{ kPa})$$

$$= 1.2 \times 10^{-5} \text{ (in mole fraction)}$$

The gas solubility at 32 °C can be found from the literature to be $C_s(32 \text{ °C}) = 1.3 \times 10^{-5}$ (in mole fraction).[26,27] Thus, we found

$$f_{(H)} = C_{i(H)}(32°C)/C_S(32°C) \approx 1.15 \text{ for water}_{(H)}$$

Table 1. Size of Interfacial Nanobubbles (INBs) in Water$_{(L)}$ at Time = 0.25 h, 14 h, and 20 h^a

size (nm)	time (h)	I	II	III	IV	V	VI	VII	VIII	IX	X	XI
H	0.25	198	128	149	80	17	22	45	48	49	58	203
	14	146	70	105	55	11	14	36	0	0	38	165
	20	150	56	105	51	0	0	35	0	0	38	164
L	0.25	901	686	777	546	194	227	375	403	415	441	966
	14	909	595	717	453	157	176	356	0	0	366	981
	20	904	464	710	424	0	0	317	0	0	300	961
R	0.25	2150	1900	2100	1900	1100	1200	1600	1700	1800	1700	2400
	14	2900	2560	2500	1900	1100	1100	1800	0	0	1800	3000
	20	2800	1950	2450	1800	0	0	1450	0	0	1200	2900

^{a}INBs (I−IV) correspond to the same INBs in Figure 2. INBs shrank primarily by reducing their heights (H) with little change in their lateral sizes (L).

Table 2. Size of Interfacial Nanobubbles (INBs) in Water$_{(H)}$ at time = 3 h and 19 h^a

size (nm)	time (h)	I	II	III	IV	V	VI	VII	VIII	IX	X	XI	XII
H	3	41	48	50	51	54	58	58	59	67	73	78	99
	19	48	56	70	62	70	73	71	66	73	79	95	119
L	3	691	763	799	812	826	816	889	825	1002	992	1157	1482
	19	733	770	855	836	876	892	898	858	968	1015	1176	1486
R	3	1469	1545	1608	1630	1596	1474	1726	1474	1920	1730	2177	2834
	19	1427	1360	1348	1432	1398	1398	1456	1428	1647	1678	1867	2384

^{a}INBs grew slightly with time with the pronounced relative increase in height.

$$f_{(L)} = C_{i(L)}(32°C)/C_S(32°C) \approx 0.92 \text{ for water}_{(L)}$$

We note that the assumption of the fully closed system used here provides the upper limit for $f_{(H)}$ and the lower limit for $f_{(L)}$ because any leakage in a supersaturated system would cause outflow of gas out of the system and vice versa.

■ RESULTS AND ANALYSES

1. Morphology of INBs in Partially Degassed Water.
Immediately after INBs were produced in the air-equilibrated water, we found that their height (H) was in the range 15−600 nm and their lateral size (L) was in the range 0.6−7 μm (Figure 1A). Figure 1B shows a typical bubble with a height of 200 nm and lateral size of 2.5 μm. After water$_{(H)}$ was replaced with water$_{(L)}$, the INBs noticeably shrank or even disappeared (Figure 2). The sizes of 11 INBs were assessed after 0.25, 14, and 20 h incubation in water$_{(L)}$, the results of which are summarized in Table 1. Some small INBs disappeared, while the others noticeably shrank between 0.25 and 14 h. More INBs disappeared from 14 to 20 h.

It was reported that, in an "air-equilibrated" water, INBs could remain for several days.[11] However, here we observed clearly that the lifetime of INBs became much shorter in water$_{(L)}$ and shrank or disappeared with a time scale of less than 1 day. This result suggests that the gas saturation level in water was critical for the lifetime of INBs. This would be also expected for larger bubbles, that is, the bubbles lose volume with the decrease of the gas saturation level in the surrounding liquid.

Table 1 shows an outstanding feature during dissolution of INBs: the height of the INBs noticeably reduced, while their lateral size remained largely *constant*. Figure 2 shows the temporal evolution of the cross-sectional profiles of four INBs, labeled as I, II, III, and IV, after 20 h incubation in water$_{(L)}$. All four INBs became considerably flatter with incubation time. While the smallest of the four bubbles (IV) noticeably shrank in the lateral direction after 14 h incubation, the middle-sized bubble (II) shrank only after 20 h incubation, and the two largest bubbles (I and III) changed little after 20 h incubation (Figure 2D and Table 1).

Furthermore, the boundary pinning of INBs was observed during growth of INBs in water$_{(H)}$. As shown in Table 2, both the height and the lateral size of INBs increased with incubation time, but the former was clearly more pronounced than the latter. This result is consistent with our previous observation that INBs grew almost exclusively in height after brief sonication.[28]

2. Laplace Pressure in Shrinking INBs.
Encouraged by the above results, we regarded INBs as pinned bubbles and analyzed the Laplace pressure and effect of the gas saturation levels on their stability. The Laplace pressure (ΔP) of a spherical-cap-shaped pinned bubble with a radius of curvature (R) can be expressed in terms of the morphological parameters shown in the schematic drawing in Figure 1B, where γ is the surface tension of water and R is the curvature radius of the bubble. For a spherical cap, $R = ((L/2)^2 + H^2)/2H$; thus

$$\Delta P = \frac{2\gamma}{R} = \frac{2\gamma}{\frac{(L/2)^2 + H^2}{2H}} = \frac{4\gamma H}{(L/2)^2 + H^2} \tag{1}$$

According to eq 1, when the lateral size (L) of a bubble is constant due to the boundary pinning, the Laplace pressure (ΔP) inside the bubble monotonically *decreases* as its height (H) *decreases* ($0 < H < L/2$). Equation 1 also shows that the Laplace pressure *increases* with the volume *increase* of the bubble with a pinned three-phase boundary, which would slow down growth of the INBs. In this scenario, the change of the Laplace pressure inside INBs should provide a negative feedback to slow down both its shrinkage and its growth. This suggests that INBs as pinned bubbles are in stark contrast to bubbles in bulk, where the Laplace pressure provides a positive feedback to accelerate bubble dissolution.

3. 1D Version of the Epstein−Plesset (E−P) Model.
To rationalize how the gas saturation level and pinning come into play in the stability of INBs, we extended the original 3D

version of the E−P model, developed by Epstein and Plesset,[29] to model the gas flow kinetics out of pinned INBs. The new model was referred to as the "1-D version of E−P model" here, as the direction of gas flow is assumed to be one-dimensional. Because INBs are very flat (the lateral dimensions are much greater than the height dimension, although figures exaggerate the height dimension relative to the lateral dimensions with the use of different scales), we assume that the directions of the gas flow are limited to those perpendicular to the bubble surface. In this model, gas number concentration in water, $c(x,t)$, as a function of time (t) and distance (x) from the bubble surface obeys the 1-D diffusion equation at a given cross section

$$\frac{\partial c}{\partial t} = D\frac{\partial^2 c}{\partial x^2} \tag{2}$$

in $x \geq 0$ and $t > 0$ ($x = 0$ is bubble surface).

With the initial and boundary conditions from Epstein−Plesset (EP)

$$c(x, t = 0) = C_i$$

$$c(x = 0, t) = c_0(t)$$

$$c(x \to \infty, t) = C_i$$

The first condition means that before diffusion starts at $t = 0$ the concentration of the gas in bulk water is uniform and equal to C_i, all the way up to the bubble surface. The second condition means that once diffusion starts ($t > 0$) the concentration of the gas in bulk water next to the bubble surface remains at the solubility of the gas (i.e., fully saturated). The third condition means that the concentration of the gas in bulk water far away from the bubble surface is maintained at C_i all the time.

If we define $u(x, t) \equiv c(x, t) - C_i$ we have

$$\frac{\partial u}{\partial t} = D\frac{\partial^2 u}{\partial x^2}$$

with the initial and boundary conditions of

$$u(x, t = 0) = 0$$

$$u(x \to \infty, t) = 0$$

$$u(x = 0, t) = c_0(t) - C_i \equiv \Delta c(t)$$

We can solve the differential equation by Laplace transform

$$U(x, s) = \int_0^\infty e^{-st}u(x, t)\,dt$$

Then the diffusion equation becomes

$$\frac{\partial^2 U}{\partial x^2} = \frac{s}{D}U$$

The solution for this equation is

$$U(x, s) = \Delta C(s)\exp(\sqrt{-s/D}\,x)$$

in which $\Delta C(s)$ is the Laplace transform of $\Delta c(t)$. Thus

$$\partial U(x, s)/\partial x = -\Delta C(s)\sqrt{s/D}\exp(-\sqrt{s/D}\,x) \tag{3}$$

Epstein−Plesset assumed that the gas concentration just outside the bubble is that of saturation, so $c_0(t) = C_s$, that is, $\Delta c(t) = [C_s - C_i] = $ const.

By solving the equation through the Laplace transform, $\Delta C(s) = [C_s - C_i]/s$, we could obtain the solution $U(x,s) = ([C_s - C_i]/s) \exp(-(s/D)^{1/2}x)$

$$\partial U(x, s)/\partial x = -\frac{[C_s - C_i]}{\sqrt{sD}}\exp(-\sqrt{s/D}\,x) \tag{4}$$

By the inverse Laplace transform

$$\partial c(x, t)/\partial x = -\frac{[C_s - C_i]}{\sqrt{\pi Dt}}\exp(-x^2/(4Dt)) \tag{5}$$

we obtain the gas flux ($J < 0$ if gas leaves bubble) as

$$J = D[\partial c/\partial x]_{x=0} = -\frac{\sqrt{D}\,[C_s - C_i]}{\sqrt{\pi t}} \tag{6}$$

The number of gas molecules in the bubble is defined as $N(t)$. Then the gas number balance equation becomes

rate of increase in $N(t)$ = gas flow into the bubble

(= area × flux)

Hence

$$\frac{dN(t)}{dt} = A_{LG}J \tag{7}$$

where the area of the liquid−gas interface, A_{LG}, is given by

$$A_{LG} = \pi\left[\left(\frac{L}{2}\right)^2 + H(t)^2\right] \tag{8}$$

In the Epstein−Plesset model it was further assumed that the bubble gas number density C_B remained constant, so the number of gas molecules was proportional to the bubble volume.[29] We used the same assumption here

$$N(t) = c_B V_G(t)$$
$$= c_B[(\pi/3)H^2(3R - H)]$$
$$= (\pi/6)c_B\left[3\left(\frac{L}{2}\right)^2 + H^2\right]H \tag{9}$$

By substituting eqs 8 and 9 into eq 7, we obtain

$$\frac{\pi}{6}c_B\frac{d}{dt}\left[\left(3\left(\frac{L}{2}\right)^2 + H(t)^2\right)H(t)\right]$$
$$= -\pi\left[\left(\frac{L}{2}\right)^2 + H(t)^2\right]\frac{\sqrt{D}\,[C_s - C_i]}{\sqrt{\pi t}} \tag{10}$$

However, since $L/2 \gg H(t)$ for INBs

$$\frac{dH}{dt} = -2\frac{(C_s - C_i)}{C_B}\sqrt{\frac{D}{\pi t}} \tag{11}$$

Solution of this differential equation by integration is

$$H(t) = H(0) - 4\frac{(C_s - C_i)}{C_B}\sqrt{\frac{Dt}{\pi}} \tag{12}$$

where D is the diffusion coefficient of air in water, C_i is the initial dissolved gas concentration in bulk water, C_s is the saturation gas concentration, C_B is the initial gas density inside the bubble (which is assumed to remain constant), and $H(0)$ is the initial height of the bubble.

The bubble lifetime, τ, can be obtained by solving eq 12 for $H(\tau) = 0$

$$\tau = \frac{\pi H^2(0)}{16D}\left(\frac{[C_s - C_i]}{C_B}\right)^{-2} \quad (13)$$

The lifetime thus depends on the gas saturation $((C_s - C_i)/C_B)$ in water and the initial thickness of the INB, $H(0)$. It also depends on the gas density inside the INB, C_B, which in turn depends on the Laplace pressure inside the INB and hence on the curvature of the interface of the INB. Thus, the lifetime implicitly includes the surface tension as well as the lateral size of the INB, L, although these quantities are assumed to be constant.

4. Comparison of the Dissolution of INBs and Free Bubbles.

We now compare the dissolution kinetics of INB in our 1-D model with that of a nanobubble of the same initial volume in bulk water that can be calculated from the original 3D E−P model. The comparison is to show how markedly different 1D INBs behave from conventional 3D NBs in bulk solution.

Figure 3 shows a comparison of the dissolution kinetics of an INB in our 1-D model and that of a spherical nanobubble in
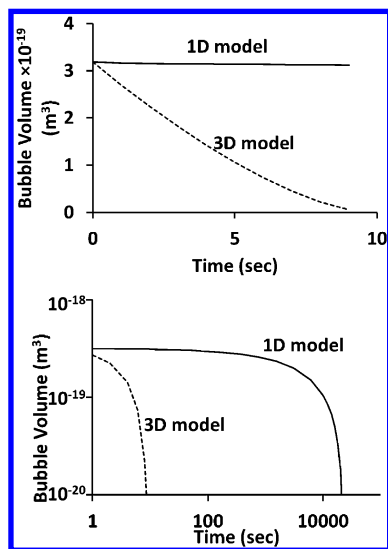

Figure 3. Comparison of dissolution dynamics of the orginal Epstein−Plesset (3-D) model and 1-D version model, both in the linear and in the logarithmic scales. Bubble had the same initial volume, and saturation level of dissolved air was 0.999. Initial volume was chosen for a typical INB of $H = 200$ nm and $L = 2$ μm.

bulk water (the original 3D E−P model). For the dissolution kinetics of an INB, we used a typical INB of $H_0 = 2 \times 10^{-7}$ m and $L = 2 \times 10^{-6}$ m as initial conditions. This corresponds to the initial volume of $V_0 = 3.18 \times 10^{-19}$ m³. The radius of curvature of the air−water interface was $R_0 = 2.6 \times 10^{-6}$ m. The surface tension of water, 0.072 N/m, was used for calculation of the initial Laplace pressure inside the INB, $2\gamma/R_0$. The initial total gas pressure inside the INB was calculated as the atmospheric pressure plus the Laplace pressure, $P_0 = (1 \times 10^5) + 2\gamma/R_0$ Pa = 1.55 atm. The solubility of air in water was about 1.5×10^{-5} in mole fraction, which equates to $C_s = 8.33 \times 10^{-4}$ mol/L. C_i, the initial concentration of air in water, was calculated by multiplying the saturation level (set as 0.999 in Figure 3) by C_s. C_B, the number density of air, was calculated

using the ideal gas equation. Conversion of the units so that C_s, C_i, and C_B have the same units yields $C_B = 0.0632$ mol/L. The diffusion coefficient of air of 2×10^{-9} m² s⁻¹ was used.

For the spherical bubble in bulk water, we used the original 3D version of the E−P model, for which D and C_B were also assumed to be constant.[29] We used the approximate solution of eq 16 of ref 29. The parameters used in eq 16 are given in eqs 12 and 13 of ref 29. In our notation, $\kappa = D$ and $\rho = C_B$; thus

$$\left(\frac{R}{R_0}\right)^2 = 1 - \left(\frac{2D(C_s - C_i)}{C_B R_0^2}\right)t \quad (14)$$

Rearrangement of eq 14 yields

$$R = \sqrt{R_0^2 - 2Dt\frac{(C_s - C_i)}{C_B}} \quad (15)$$

The initial radius of a spherical nanobubble in bulk water, which has the same initial volume as that of the INB of $V_0 = 3.18 \times 10^{-19}$ m³, is calculated to be $R_0 = (3V_0/4\pi)^{1/3} = 4.24 \times 10^{-7}$ m (see above). The initial total gas pressure inside a nanobubble was calculated as 1 atm plus the Laplace pressure, $P_0 = (1 \times 10^5) + 2\gamma/R_0$ Pa = 4.4 atm. We used the same C_s, C_i, and diffusion coefficient of air as those used for the INB calculations above. C_B, calculated using the ideal gas equation, was found to be 0.179 mol/L.

It can be seen that deflation of an INB was much slower than that of a spherical bubble of the same volume. The lifetime of INBs was sensitive to the saturation level, especially when the dissolved gas was close to saturation. For example, the lifetime of a typically sized INB varied from about 200 s at a saturation level of 0.99 to more than 200 000 s at a saturation level of 0.9999, while the lifetime of a bulk nanobubble of the same initial volume varied from about 1 to 100 s in the same span. Nevertheless, this does not alter the main conclusion that the lifetime of a pinned INB remained many orders of magnitude longer than that of a spherical bubble of the same initial volume in bulk water for a given saturation level of gas.

One might consider what will happen in the case where $C_i = C_s$, i.e., when the saturation level of air in the surrounding water is exactly at saturation. As follows from eq 5, in that case the gradient of dissolved gas concentration should be zero everywhere in the bulk of water regardless of whether a bubble is present in the liquid or not. Moreover, the diffusion flow is zero as well (eq 6), and the bubble should be stationary (eqs 11 and 12). This seems contradictive to the observation that the nanobubble height H slightly grows with time in air-equilibrated water used in the experiments. However, we stress that the "air-equilibrated water" refers to being saturated at room temperature but effectively supersaturated at the temperature for imaging (up to P/P_0 of 1.15, not $P/P_0 = 1$). Therefore, INBs are expected to grow. Theoretically, if it were possible to achieve $P/P_0 = 1$, then one would expect stationary bubbles. Experimentally it has been impossible for us to create such an exactly saturated condition, especially given that it is so sensitive to minute variation from 1, as we mentioned above "the lifetime of a typically sized INB varied from about 200 s at a saturation level of 0.99 to more than 200 000 s at a saturation level of 0.9999".

5. Further Remarks on the Stability of INBs.

Although this work cannot resolve all the puzzles for the stability of INBs, we would like to draw the readers' attention to the following three points in order to reconcile the "disagreement" between

the experimentally observed long lifetimes and theoretical predictions.

First, the term "nano" in INB (interfacial nanobubble) often refers only to its height. The mean radius of curvature of an INB is usually larger than a micrometer. Second, for a given initial volume, INBs with a *pinned boundary* dissolve much slower than a bubble in bulk water. Third, the gas saturation level is very important but difficult to control and characterize experimentally. It is influenced by many factors, such as the gas compositions, pressure fluctuations, and temperature (and the exothermic mixing of different solvents during the solvent exchange procedure). Our calculation shows that an increase of 0.01 in the saturation level can easily extend the bubble lifetime by a factor of 1000, while a temperature change of 1 °C can result in variation of more than 0.01 in the saturation level. As such, the long lifetime of INBs can be rationalized, to a large extent, by the pinning-enhanced sensitivity to the saturation level of dissolved gas in water according to our 1D version of the E−P models.

Our final comments on the role of the pinning are that it may slow down the kinetics of the Ostwald ripening among differently sized INBs. As shown in Figure 1A and in many other AFM images in the literature, the size distributions of as-prepared INBs are always polydispersed. In this case, the Ostwald ripening was expected to occur with time to minimize the free energy in the system, i.e., larger INBs were expected to grow with time at the expense of smaller ones. Although the kinetics of the Ostwald ripening is complex and influenced by several factors,[30] it is theoretically expected to be facilitated by the large gas pressures inside INBs. However, experimentally, Ostwald ripening of as-prepared INBs was found to be minimal in the air-equilibrated water. This observation could also be explained by our current findings that both growth and shrinking of INBs are slowed down due to the pinning of their boundaries.[31]

CONCLUSIONS

This work shows that the pinning of the three-phase boundaries of INBs and the saturation level of the dissolved gas in the surrounding water were the two critical contributions to the long lifetimes of INBs. Due to this pinning, the Laplace pressure inside the INBs decreased during dissolution and increased during growth, opposite of what was expected for small bubbles floating in bulk water. At the same time, the lifetimes of INBs are highly sensitive to the gas saturation level in the surrounding water. A small change in the gas saturation level that could arise from temperature fluctuations would dramatically influence the lifetimes of INBs. The focus of our current research is to understand the origin of the boundary pinning.

AUTHOR INFORMATION

Corresponding Author
*Email: xuehuaz@unimelb.edu.au.

Notes
The authors declare no competing financial interest.

ACKNOWLEDGMENTS

REFERENCES

(1) Poynor, A.; Hong, L.; Robinson, I. K.; Granick, S.; Zhang, Z.; Fenter, P. A. How Water Meets a Hydrophobic Surface. *Phys. Rev. Lett.* **2006**, *97*, 266101.
(2) Mezger, M.; Reichert, H.; Schoder, S.; Okasinski, J.; Schroder, H.; Dosch, H.; Palms, D.; Ralston, J.; Honkimaki, V. High-resolution in situ X-ray Study of the Hydrophobic Gap at the Water-Octadecyl-trichlorosilane Interface. *Proc. Natl. Acad. Sci. U.S.A.* **2006**, *103*, 18401−18404.
(3) Meyer, E. E.; Rosenberg, K. J.; Israelachvili, J. Recent Progress in Understanding Hydrophobic Interactions. *Proc. Natl. Acad. Sci. U.S.A.* **2006**, *103*, 15739−15746.
(4) Wu, Z. H.; Zhang, X. H.; Zhang, X. D.; Sun, J. L.; Dong, Y. M.; Hu, J. In situ AFM observation of BSA adsorption on HOPG with nanobubble. *Chinese Sci. Bull.* **2007**, *14*, 1913−1919.
(5) Christenson, H. K.; Claesson, P. M. Direct measurements of the force between hydrophobic surfaces in water. *Adv. Colloid Interface Sci.* **2001**, *91*, 391−436.
(6) Carambassis, A.; Jonker, L.; Attard, P.; Rutland, M. Forces Measured between Hydrophobic Surfaces due to a Submicroscopic Bridging Bubble. *Phys. Rev. Lett.* **1998**, *80*, 5357−5360.
(7) de Gennes, P. G. On fluid/wall slippage. *Langmuir* **2002**, *18*, 3413−3414.
(8) Hampton, M. A.; Nguyen, A. V. Nanobubbles and the Nnanobubble Bridging Capillary Force. *Adv. Colloid Interface Sci.* **2010**, *154*, 30−55.
(9) Zhang, X. H.; Kumar, A.; Scales, P. J. Effects of Solvency and Interfacial Nanobubbles on Surface Forces and Bubble Attachment at Solid Surfaces. *Langmuir* **2011**, *27*, 2484−2491.
(10) Tyrrell, J. W. G.; Attard, P. Images of Nanobubbles on Hydrophobic Surfaces and Their Interactions. *Phys. Rev. Lett.* **2001**, *8717*, 176104.
(11) Zhang, X. H.; Quinn, A.; Ducker, W. A. Nanobubbles at the Interface between Water and a Hydrophobic Solid. *Langmuir* **2008**, *24*, 4756−4764.
(12) Ljunggren, S.; Eriksson, J. C. The Lifetime of a Colloid-Sized Gas Bubble in Water and the Cause of the Hydrophobic Attraction. *Colloids Surf. A* **1997**, *130*, 151−155.
(13) Zhang, X. H.; Khan, A.; Ducker, W. A. A Nanoscale Gas State. *Phys. Rev. Lett.* **2007**, *98*, 136101.
(14) Das, S. Effect of Impurities in the Description of Surface Nanobubbles: Role of Nonidealities in the Surface Layer. *Phys. Rev. E* **2011**, *83*, 066315.
(15) Das, S.; Snoeijer, J. H.; Lohse, D. Effect of Impurities in Description of Surface Nanobubbles. *Phys. Rev. E* **2010**, *82*, 056310.
(16) Attard, P. Nanobubbles and the Hydrophobic Attraction. *Adv. Colloid Interface Sci.* **2003**, *104*, 75−91.
(17) Ducker, W. A. Contact Angle and Stability of Interfacial Nanobubbles. *Langmuir* **2009**, *25*, 8907−8910.
(18) Zhang, X. H.; Uddin, M. H.; Yang, H. J.; Toikka, G.; Ducker, W.; Maeda, N. Effects of Surfactants on the Formation and the Stability of Interfacial Nanobubbles. *Langmuir* **2012**, *28*, 10471−10477.
(19) Brenner, M. P.; Lohse, D. Dynamic Equilibrium Mechanism for Surface Nanobubble Stabilization. *Phys. Rev. Lett.* **2008**, *101*, 214505.
(20) Seddon, J. R. T.; Zandvliet, H. J. W.; Lohse, D. Knudsen Gas Provides Nanobubble Stability. *Phys. Rev. Lett.* **2011**, *107*, 116101.
(21) Borkent, B. M.; de Beer, S.; Mugele, F.; Lohse, D. On the Shape of Surface Nanobubbles. *Langmuir* **2010**, *26*, 260−268.
(22) Song, B.; Walczyk, W.; Schonherr, H. Contact Angles of Surface Nanobubbles on Mixed Self-Assembled Monolayers with Systematically Varied Macroscopic Wettability by Atomic Force Microscopy. *Langmuir* **2011**, *27*, 8223−8232.
(23) Lou, S. T.; Ouyang, Z. Q.; Zhang, Y.; Li, X. J.; Hu, J.; Li, M. Q.; Yang, F. J. Nanobubbles on Solid Surface Imaged by Atomic Force Microscopy. *J. Vac. Sci. Technol. B* **2000**, *18*, 2573−2575.

(24) Zhang, X. H.; Zhang, X. D.; Lou, S. T.; Zhang, Z. X.; Sun, J. L.; Hu, J. Degassing and Temperature Effects on the Formation of Nanobubbles at the Mica/Water Interface. *Langmuir* **2004**, *20*, 3813–3815.

(25) Zhang, X. H.; Maeda, N.; Craig, V. S. J. Physical Properties of Nanobubbles on Hydrophobic Surfaces in Water and Aqueous Solutions. *Langmuir* **2006**, *22*, 5025–5035.

(26) In *Gas solubilities*, 1st ed.; Gerrard, W., Ed.; Pergamon Press: New York, 1980.

(27) In *CRC Handbook of Chemistry and Physics*, 86th ed.; Lide, D. R., Ed.; Taylor and Francis Group LLC: New York, 2006.

(28) Brotchie, A.; Zhang, X. H. Response of Interfacial Nanobubbles to Ultrasound Irradiation. *Soft Matter* **2011**, *7*, 265–269.

(29) Epstein, P. S.; Plesset, M. S. On the Stability of Gas Bubbles in Liquid-Gas Solutions. *J. Chem. Phys.* **1950**, *18*, 1505–1509.

(30) Voorhees, P. W. The Theory of Ostwald Ripening. *J. Stat. Phys.* **1985**, *38*, 231–252.

(31) Jones, S. F.; Evans, G. M.; Galvin, K. P. Bubble Nucleation from Gas Cavities - a Review. *Adv. Colloid Interface Sci.* **1999**, *80*, 27–50.